

# Spherical-Harmonic Distribution Analysis of Coronae in Relation to Volcanic Features on Venus

Wesley S. Tucker<sup>1</sup> and Andrew J. Dombard<sup>2</sup>

<sup>1</sup>University of Illinois Chicago

<sup>2</sup>University of Illinois at Chicago

November 22, 2023

## Abstract

Venus boasts an abundance of volcano and volcano-like structures. Synthetic aperture radar images of the surface have revealed extensive evidence of volcanism, including lava flows and edifices. Volcanic activity is further supported by crater statistics, and analysis of topography and gravity data. Unique to Venus, coronae are quasi-circular, volcano-tectonic features exhibiting diverse volcanic characteristics. Despite this, volcanism is often under-represented in formation models. We identify a new subset of coronae that display topographic change subsequent to the emplacement of lava flows within their fracture annuli, pointing to the critical role of volcanism in the formation of these coronae. Through spherical-harmonic distribution analysis, we find that this new subset is spatially related to the full coronae database, pointing to an intrinsic process of coronae formation. Furthermore, coronae exhibit strong correlations and similar spectral shapes at low spherical harmonic degrees with large volcanoes, suggesting a shared geodynamic origin. Our findings underscore the pivotal role of volcanism in coronae formation and highlight the need for future research that integrates magmatic processes into geophysical models.

## Hosted file

979756\_0\_art\_file\_11599163\_s4870d.docx available at <https://authorea.com/users/633157/articles/687783-spherical-harmonic-distribution-analysis-of-coronae-in-relation-to-volcanic-features-on-venus>

## Hosted file

979756\_0\_supp\_11599164\_s4870s.docx available at <https://authorea.com/users/633157/articles/687783-spherical-harmonic-distribution-analysis-of-coronae-in-relation-to-volcanic-features-on-venus>



## 12 **Abstract**

13 Venus boasts an abundance of volcano and volcano-like structures. Synthetic aperture radar  
14 images of the surface have revealed extensive evidence of volcanism, including lava flows and  
15 edifices. Volcanic activity is further supported by crater statistics, and analysis of topography  
16 and gravity data. Unique to Venus, coronae are quasi-circular, volcano-tectonic features  
17 exhibiting diverse volcanic characteristics. Despite this, volcanism is often under-represented in  
18 formation models. We identify a new subset of coronae that display topographic change  
19 subsequent to the emplacement of lava flows within their fracture annuli, pointing to the critical  
20 role of volcanism in the formation of these coronae. Through spherical-harmonic distribution  
21 analysis, we find that this new subset is spatially related to the full coronae database, pointing to  
22 an intrinsic process of coronae formation. Furthermore, coronae exhibit strong correlations and  
23 similar spectral shapes at low spherical harmonic degrees with large volcanoes, suggesting a  
24 shared geodynamic origin. Our findings underscore the pivotal role of volcanism in coronae  
25 formation and highlight the need for future research that integrates magmatic processes into  
26 geophysical models.

## 27 **Plain Language Summary**

28 Venus's surface has a large number of volcanoes and features with characteristics similar to  
29 volcanoes. Radar imagery of the surface reveals signs of volcanism such as lava flows and  
30 volcanically built mountains. A unique volcanic feature, found only on Venus, are coronae,  
31 which have circular fractures and various types of associated volcanic activity. Explanations of  
32 how coronae form often do not consider the role of volcanic activity. In our study, we identify a  
33 new group of coronae that have undergone changes in topography after lava erupted and flowed  
34 over them, which has been interpreted as volcanism having a central role in corona formation.  
35 The locations of this subset of coronae on the surface fits well with all other coronae, suggesting  
36 the processes that caused this topographic change occur throughout the corona population and  
37 are a basic part of how all coronae form. Additionally, we find that coronae have a similar  
38 pattern on the surface to large volcanoes, which indicates a shared, volcanically based origin.  
39 Our work shows that in order to better understand coronae, we need to consider the role of  
40 volcanism in their formation.

## 41 **1 Introduction**

42 NASA's Magellan spacecraft, with its single radar system, provided data covering nearly  
43 the entire surface of Venus. The high-resolution ( $\sim 75$  m/pix) synthetic aperture radar (SAR) data  
44 presented a detailed view of the surface, enabling the identification of extensive volcanic features  
45 beyond the capabilities of the preceding Venera 15/16 missions. These improved data revealed a  
46 more extensive range of volcanoes, with diameters from less than 1 km to over 100 km (e.g.,  
47 Guest et al., 1992; Head et al., 1992), and provided a more detailed view of the intriguing  
48 volcano-tectonic structures known as coronae (e.g., Squyres et al., 1992; Stofan et al., 1992).  
49 Many hypotheses have been proposed regarding the formation and evolution of coronae, and the  
50 debate has continued since the early days of the Magellan mission (e.g., Copp et al., 1998;

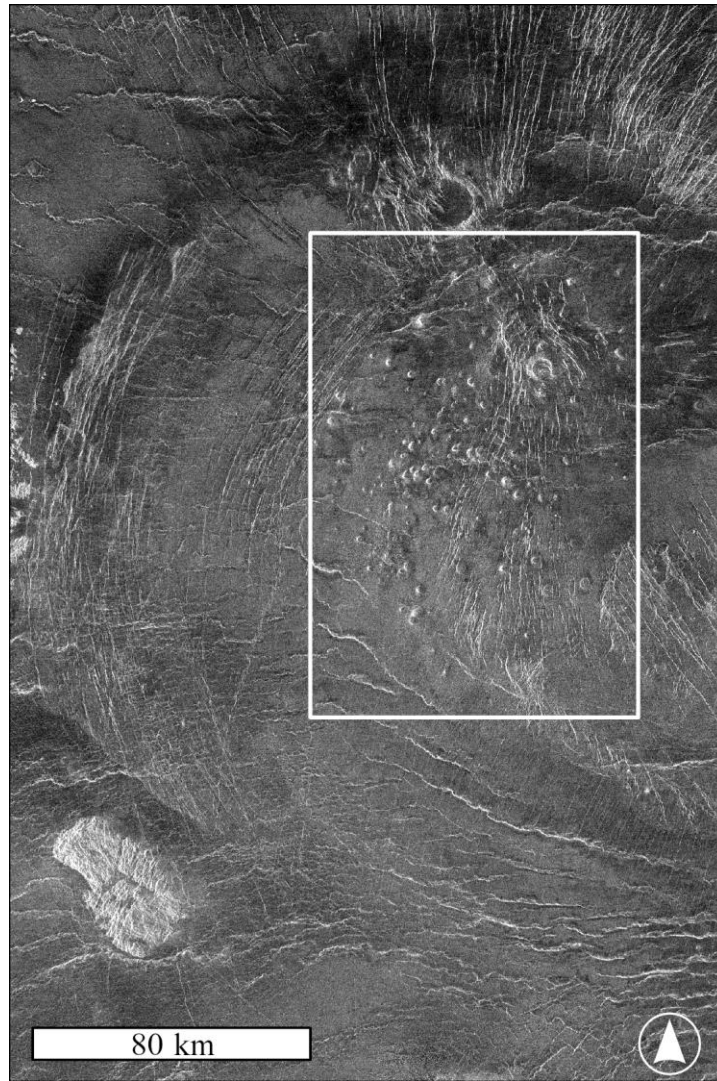
51 Davaille et al., 2017; DeLaughter & Jurdy, 1999; Dombard et al., 2007; Gerya, 2014; Gülcher et  
52 al., 2021; Hoogenboom & Houseman; 2006; Janes & Squyres, 1995; Koch & Manga; 1996;  
53 Lang and López, 2015; Smrekar & Stofan, 1997).

54 Numerous volcanoes and volcano-like structures are scattered across the surface of  
55 Venus. Using Venera 15/16 data, volcanoes were initially binned into three size classes: small,  
56 intermediate, and large (e.g., Slyuta, 1990; Slyuta & Kreslavsky, 1990). Following NASA's  
57 Magellan mission, this classification system continued, in part for consistency (e.g., Head et al.,  
58 1992), but also for convenience as the individual SAR swaths were roughly 20 km wide during  
59 the early stages of the mission (Crumpler et al., 1997). Further, these divisions were consistent  
60 with the cumulative size distribution of the 1195 volcanoes identified by Crumpler et al. (1997).  
61 Roughly half of the edifices identified in that study had diameters between 20 km and 100 km.

62 A recent survey substantially expanded on the number of volcanoes. Hahn & Byrne  
63 (2023) identified ~85,000 edifices. To skirt away from the arbitrariness of early size binning, the  
64 authors employed “mixture modeling” to determine if there are discrete populations of volcanoes  
65 based on their diameters and found two distinct exponential distributions when splitting the data  
66 into two sets: volcanoes between 5 km and 63 km (diameters were not measured for volcanoes  $\leq$   
67 5 km) and volcanoes  $>$  63 km (see Figure 6 of Hahn & Byrne, 2023).

68 A specific focus of Venusian volcano studies has been on shield volcanoes, which make  
69 up a significant percentage of the observed edifices. Early observations from Venera 15/16 data  
70 noted the high number of small shield volcanoes, ~22,000, with just 25% of the surface being  
71 imaged at the time (Aubele & Slyuta, 1990). Shield volcanoes often occur in relatively high  
72 spatial concentrations, termed “shield fields” or “volcanic fields” (Figure 1). The most recent  
73 catalogue of volcanoes included 566 volcanic fields (Hahn & Byrne, 2023). Shield volcanoes  
74 display small topographic signatures and diameters of 20 km or less. They are proposed to result  
75 from distinct crustal melt sources that are unable to supply magma at rates sufficient for building  
76 a single edifice (Guest et al., 1991; Head et al., 1992; Ivanov et al., 2017; Thomas & Lang,  
77 2016).

78



79

80

81 **Figure 1.** Magellan SAR image (75 m/pix) of a cluster of shield volcanoes (white box) from a  
82 volcanic field identified by Hahn & Byrne (2023) within Belet-ili Corona (6°N, 20°E). Circular,  
83 radar bright spots represent individual shield volcanoes.

84

85 Venus hosts more than 500 coronae, quasi-circular volcano-tectonic features (Stofan et  
86 al., 2001a). Being unique to Venus, their existence might provide critical insights into the  
87 differences between Earth's and Venus's lithospheres. For instance, they may contribute  
88 significantly to the heat loss budget on Venus, which is difficult to explain due to the lack of  
89 plate tectonics (e.g., Smrekar & Stofan, 1997; Smrekar et al., 2018).

90 The term “corona” refers to the features’ morphology, specifically their circular structure  
91 composed of concentric fracture and ridge annuli (Barsukov et al., 1986). A survey of Magellan  
92 SAR images by Stofan et al. (2001a) significantly expanded the corona database to roughly its  
93 current size (see section 2.1). Though initially classified based solely on morphologic  
94 characteristics, a more comprehensive understanding of coronae emerges from four critical  
95 observations: an annulus of tectonic structures, varied and complex topography, a wide range of  
96 diameters, and associated volcanism (e.g., Dombard et al., 2007; Tucker & Dombard, 2023a).

97 The critical observations underscore the diverse characteristics exhibited by coronae. For  
98 example, the size of the fracture annulus within coronae varies from 10 km to over 150 km  
99 (Stofan et al., 1992). Furthermore, the topographic signatures of coronae are diverse and  
100 complex. Despite this, they have been categorized into nine distinct classifications (Smrekar &  
101 Stofan, 1997; Stofan et al., 1997, 2001). Coronae cover a wide range of diameters, ranging from  
102 as small as 60 km to as large as 2600 km for Artemis Corona. However, Artemis Corona is  
103 approximately 1600 km wider than the next largest corona, Heng-O, and it may have formed  
104 through a completely different set of processes (e.g., Davaille et al., 2017; Hansen, 2002;  
105 McKenzie et al., 1992; Sandwell & Schubert, 1992).

106 Last, coronae are closely associated with various forms and intensities of volcanism.  
107 Large lava flow fields, of the order of terrestrial flood basalts, have been linked to sources  
108 associated with coronae (e.g., Roberts & Head, 1993). Individual lava flows are also observable  
109 within and radiating from the fracture annuli (e.g., Tucker & Dombard, 2023a). Additionally,  
110 other volcanic edifices, such as tholi or small shield volcanoes, are often found within or on  
111 corona annuli (e.g., Lang & López, 2015; Roberts & Head, 1993; Russell & Johnson, 2021; and  
112 cf. Fig. 1).

113 Venus has a relative lack of impact craters when compared to other bodies in the solar  
114 system, apart from Earth, indicating a youthful surface and a history of resurfacing. This finding,  
115 coupled with the presence of abundant volcanic features, raises questions regarding the current  
116 level of geologic activity on Venus. Surveys of the crater population have identified  
117 approximately 900 impact structures (e.g., Herrick et al., 1997; Phillips et al., 1992; Schaber et  
118 al., 1992) with a spatial distribution that cannot be distinguished from a random population (e.g.,  
119 Hauck et al., 1998; Phillips et al., 1992; Strom et al., 1994). The seemingly random distribution

120 of craters (see Figure 2 of Herrick et al., 2023) has led to an inferred global surface age ranging  
121 from approximately 300 to 800 Myr (e.g., Hauck et al., 1998; McKinnon et al., 1997). Venus  
122 does not show major effects of erosion (Arvidson et al., 1992), and thus the only explanation for  
123 the lack of cratering is either volcanism or tectonism (Hauck et al., 1998). Two hypotheses have  
124 emerged to explain Venus's cratering: a catastrophic resurfacing model (Schaber et al., 1992;  
125 Strom et al., 1994) or a continuous (or equilibrium) resurfacing model (Phillips et al., 1992),  
126 although, the catastrophic resurfacing model is no longer thought to be valid (e.g., Guest &  
127 Stofan, 1999; Hauck et al., 1998; Herrick & Sharpton, 2000). On this basis, Venus could be  
128 volcanically active today.

129         Indeed, several studies have presented intriguing findings of potential recent volcanism.  
130 For instance, thermal emission data from the Visible and Infrared Thermal Imaging Spectrometer  
131 (VIRTIS) on the European Space Agency's Venus Express spacecraft revealed emissivity  
132 anomalies in lava flows in the Themis, Imdr, and Dione Regiones, all of which are suspected  
133 areas of hotspot volcanism. The absence of surface weathering in these regions suggests that  
134 these lava flows could be as young as 250,000 years (Smrekar et al., 2010). Most recently,  
135 Herrick and Stanley (2023) observed a change in vent geometry of a shield volcano between two  
136 Magellan image cycles. The first image was interpreted as a drained volcanic vent, which  
137 appeared to refill and form a lava lake by the time of the subsequent imaging cycle.

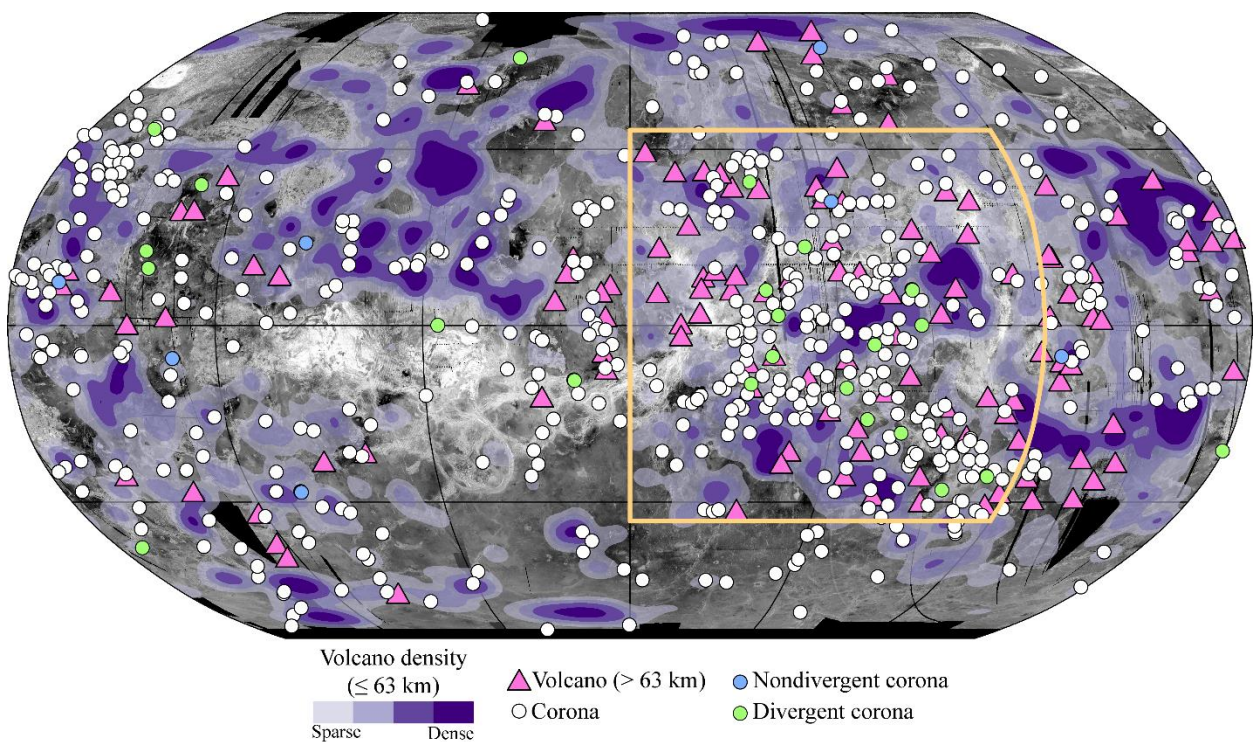
138         Studies of gravity and topography data have also provided insights into the activity states  
139 of volcanoes and coronae on Venus. The occurrence of uncompensated geoid highs in Atla, Beta,  
140 and Eistla Regiones have been interpreted as areas underlain by active mantle plumes (e.g.,  
141 Anderson & Smrekar, 2006; Grimm & Phillips, 1992; Smrekar, 1994; Stofan et al., 1995).  
142 Johnson and Richards (2003) identified coronae as candidates for potential current activity based  
143 on their compensated state. Dombard et al. (2007) further examined the gravity and topography  
144 of coronae in the BAT region, concluding that some of these features are likely currently  
145 underlain by an impinged thermal due to positive topography and geoid anomalies coinciding  
146 with negative Bouguer anomalies.

147         A connection between the topographic signatures of coronae and their activity states has  
148 also been proposed (e.g., Smrekar & Stofan, 1997). Gülcher et al. (2020) compared the  
149 topographic signatures generated by their three-dimensional thermomechanical simulations to

150 the topography of existing coronae. They concluded that 37 coronae were likely active as their  
 151 topography matched the model's plume-lithosphere interaction stages. However, these methods  
 152 primarily assume that mantle upwelling and subsurface solid-state flow influence corona  
 153 morphology and formation. In contrast, other volcanic-related processes, such as magmatic  
 154 loading (e.g., Dombard et al., 2007), collapsing magma reservoirs (e.g., Lang & López, 2015), or  
 155 volcanic construction (e.g., McGovern et al., 2013), could be responsible for coronae formation.

156 It is well established that both coronae and volcanoes show spatial clustering in the BAT  
 157 region (e.g., Hahn & Byrne, 2023; Head et al., 1992; Squyres et al., 1993; Stofan et al., 1992,  
 158 1995) (Figure 2). Their distribution, along with their relationship to topography and gravity, may  
 159 provide insights into mantle flow dynamics, and formation mechanisms.

160



162

162 **Figure 2.** Global distribution of volcanoes and corona subsets on Venus. Volcanoes with  
 163 diameters less than 63 km (N=84,894) are displayed using a kernel density estimate with a 500  
 164 km search radius (Silverman, 1986). The map is centered on 180° in Robinson projection with a  
 165 thrice compressed (~2025 m/pixel) Magellan SAR image (C3-MIDR) base layer. The yellow  
 166 outline is the Beta-Atla-Themis (BAT) region. For dataset descriptions, see section 2.

167

168 In this study, we explore the volcanic nature of coronae in greater detail. We identify a  
169 new subset of coronae that have undergone topographic changes within the fracture annuli since  
170 the emplacement of lava flows. This phenomenon, previously described by Tucker and Dombard  
171 (2023a) in detail at Atete and Aruru Coronae, suggests a magmatic influence on corona  
172 topography. To extend our understanding, we employ spatial analysis techniques and spherical  
173 harmonics to investigate the global distribution and characteristics of volcanoes, coronae, and  
174 subsets of these data. We focus on the interplay between coronae and volcanoes, with a specific  
175 emphasis on the role of volcanic processes in the formation of coronae. Through our findings, we  
176 aim to underscore the significance of coronae in our understanding of the volcanic processes  
177 shaping Venus's surface and to reiterate the inherently volcanic nature of coronae.

## 178 **2 Data and Methods**

179 In our spherical harmonic analysis, we utilize a diverse selection of datasets. These  
180 include comprehensive catalogues of both volcanoes and coronae. In addition, we analyze  
181 specific subsets from these catalogues that have been compiled by previous studies. We also  
182 analyze a novel subset of coronae, identified for this work, characterized by lava flows within the  
183 fracture annuli that diverge from the modern downhill direction. In addition to the datasets  
184 discussed below, we use spherical harmonic coefficients from models of topography  
185 (VenusTopo719) (Wieczorek, 2015) and gravity (MGNP180U) (Konopliv et al., 1999).

### 186 **2.1 Compiled datasets**

187 A contemporary survey of volcanoes on Venus identified 85,021 volcanic features (Hahn  
188 & Byrne, 2023). The authors catalogued volcanoes into three diameter bins:  $< 5$  km (small), 5 to  
189 100 km (intermediate), and  $> 100$  km (large). Of these, the majority (99%) were less than 5 km in  
190 diameter, while 729 were intermediate sized, and 118 were larger than 100 km. Moreover, Hahn  
191 and Byrne (2023) identified 566 clusters of shield volcanoes, which they termed volcanic fields,  
192 containing shield volcanoes with diameters of 20 km or less. Hahn and Byrne (2023) defined the  
193 volcano size bins to aid in the mapping and measuring of edifices. Volcanoes  $\leq 5$  km were  
194 marked as point features, while the extents of volcanoes  $> 5$  km were digitized, and their  
195 diameters were calculated. However, for their spatial analysis (see Figure 7 of Hahn & Byrne,  
196 2023), the authors classified volcanoes into those  $\leq 63$  km and those  $> 63$  km (see section 1). To  
197 be consistent with this modern catalogue of volcanoes, we will utilize these two size bins for our

198 subsets of the volcano catalogue. Notably with a minimum corona diameter of ~60 km, all  
199 coroneae are in the size range of large volcanoes.

200 We analyze coroneae on the surface of Venus by combining the Type 1 and Type 2 corona  
201 dataset from Stofan et al. (2001a) and the Venus nomenclature database from the USGS  
202 ([planetarynames.wr.usgs.gov](http://planetarynames.wr.usgs.gov)). To further refine our analysis, we incorporate a subset of the  
203 combined corona database of coroneae with lava flows that diverge from the downslope direction.

## 204 2.2 Corona associated divergent lava flows

205 Building on our preliminary work on Aruru and Atete Coroneae and using the same  
206 methodology (Tucker & Dombard, 2023a), we have identified coroneae with lava flows within  
207 their fracture annuli that diverge from the modern downhill slope direction in the combined  
208 corona dataset. Full resolution (~75 m/pix) Magellan synthetic aperture radar (SAR) images are  
209 imported into ESRI ArcMap and stretched to enable the identification of discrete lobate and  
210 digitate flow features. At coroneae with suitable flow features, flow centerlines are mapped, and  
211 the azimuthal orientation is determined using the start and end points.

212 To determine if the lava flows follow the modern topography, the line azimuth is  
213 compared to the regional slope facing direction (i.e., aspect). A 25 km buffer is placed around the  
214 center point of each flow line, and the mean regional aspect is determined for the buffer area.  
215 Aspect rasters are derived from Magellan global topographic data records (GTDR), and where  
216 available, stereo-derived digital elevation models from Herrick (2020). Comparing the flow line  
217 azimuth to the regional aspect provides data on changes in topography since the flows were  
218 emplaced. Two new subsets of corona are recorded: coroneae with intra-annular divergent flows  
219 and coroneae without intra-annular divergent flows. If the number of mapped flows that diverge  
220 from the downhill direction is twice the number of mapped flows that do not have flow  
221 divergence, we consider that corona as one with divergent flows. To determine the appropriate  
222 cutoff for classifying coroneae based on divergent and nondivergent lava flows, we analyze  
223 coroneae exhibiting both flow types (i.e., ignoring coroneae with only divergent lava flows). A  
224 predominant cluster is present around a ratio of 1, indicating a near-equivalent presence of both  
225 flow types. Additionally, a Kernel Density Estimate (KDE) analysis produces a pronounced peak  
226 near this ratio, with the density decreasing for higher ratios. Therefore, we consider a cutoff at a

227 ratio of 2 to be statistically and contextually apt for distinguishing between coronae with both  
 228 flow types and those where divergent flows prevail.

229 A total of 72 coronae, a clear subset of the total coronae population, had visible flows in  
 230 their interiors; however, 42 of those had either too few flow units or flows without discernable  
 231 margins. Divergent flows were identified in 24 corona interiors, while 6 did not have divergent  
 232 lava flows (Figure 2) (Supporting Information Table S1). For simplicity, we will refer to a  
 233 corona as either divergent or nondivergent when referring to coronae with lava flows that either  
 234 diverge or do not diverge from the modern downhill direction.

### 235 2.3 Spherical harmonic analysis

236 To examine the distribution of coronae that have undergone topographic change, we use  
 237 spectral analysis. Based on spherical harmonics, information about the wavelength that best  
 238 describes the distribution can be discerned via power spectra. Spherical harmonic analysis is a  
 239 useful tool for assessing the correlations and anticorrelations of global data subsets. Using this  
 240 method will allow for comparison of the full corona dataset with the global volcano database and  
 241 subsets of the corona database described above. Further, spectra of these data will be compared  
 242 to long-wavelength features represented by continuous data such as gravity and topography.

243 The fully normalized spherical harmonic expansions of the distribution are given by  
 244 (Johnson & Richards, 2003; Kirchoff et al., 2011)

$$245 \quad f_{lm}(\theta, \phi) = P_l^m(\cos \theta)(c_{lm} \cos m\phi + s_{lm} \sin m\theta), \quad (1)$$

246 where  $\phi$  is the longitude,  $\theta$  is the colatitude, and  $P_l^m$  is the associated Legendre polynomial of  
 247 degree  $l$  and order  $m$ . The cosine and sine coefficients,  $c_{lm}$  and  $s_{lm}$ , are determined by projecting  
 248 the locations of the features in the dataset onto a particular spherical harmonic:

$$249 \quad c_{lm} = \sqrt{\frac{(2-\delta_{0m})(2l+1)(l-m)!}{4\pi(l+m)!}} \sum_{n=1}^N P_l^m(\cos \theta_n) \cos m\phi_n \quad (2a)$$

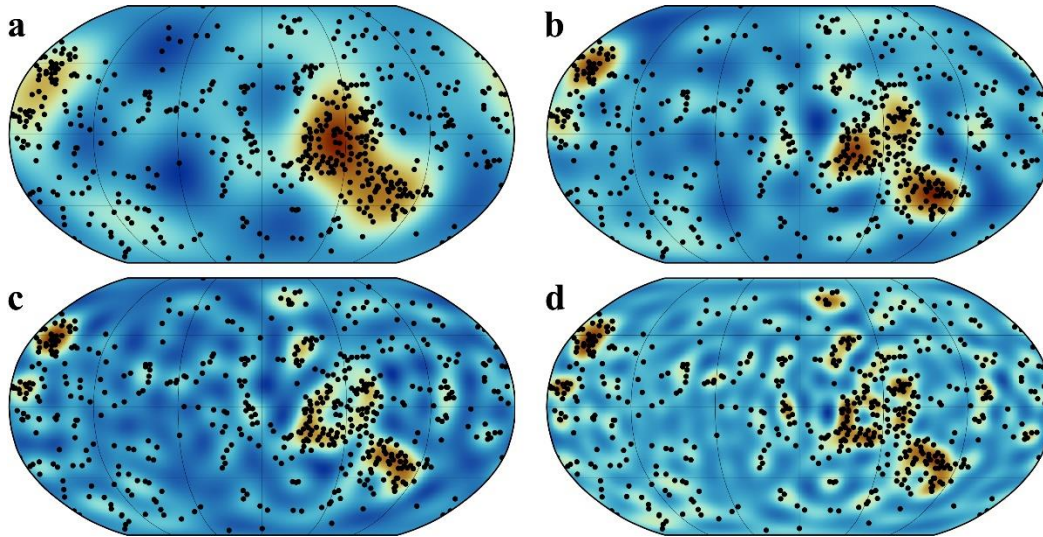
$$250 \quad s_{lm} = \sqrt{\frac{(2-\delta_{0m})(2l+1)(l-m)!}{4\pi(l+m)!}} \sum_{n=1}^N P_l^m(\cos \theta_n) \sin m\phi_n, \quad (2b)$$

251 where  $N$  is the total number of features (coronae or volcanoes) in the dataset; in this definition,  
 252 the spherical harmonics are fully normalized. The Kronecker delta function,  $\delta_{lm}$ , is

253 
$$\delta_{0m} = \begin{cases} 1, & m = 0, \\ 0, & m \neq 0. \end{cases} \quad (3)$$

254 We use a maximum degree  $l = 20$  for the expansion, which follows previous spherical harmonic  
 255 analysis on Venus (e.g., Johnson & Richards, 2003). Figure 3 illustrates the relationship between  
 256 spherical harmonic coefficients and the location of the features at several spherical harmonic  
 257 degrees.

258



259

260 **Figure 3.** Robinson projected maps showing spherical harmonic representations of the full  
 261 corona database truncated at (a)  $l = 5$ , (b)  $l = 10$ , (c)  $l = 15$ , and (d)  $l = 20$ . Black dots are  
 262 locations of coronae from the combined corona database. Hot colors (red) indicate relatively  
 263 more dense concentrations of coronae and cool colors (blue) are less dense. All maps are  
 264 centered at  $180^\circ\text{E}$ .

265

266 The spectral power is normalized for the number of features in a distribution, and with  
 267 this normalization, will appear white for random distributions (Ribe de Valpine, 1994; Richards  
 268 et al., 1988; Kirchoff et al., 2011):

269 
$$S_l = \frac{4\pi}{N(2l+1)} \sum_{m=0}^l (c_{lm}^2 + s_{lm}^2). \quad (4)$$

270 Additionally, we check for randomness of the features by comparing their spectra to  
 271 randomly generated latitude and longitude points on a sphere. Over 10,000 iterations, random  
 272 latitude-longitude points are generated for the number of samples in the dataset of interest. In

273 each iteration, the latitudes and longitudes of points are randomly generated following a uniform  
 274 distribution on a sphere. The transformation functions  $\theta = 2\pi u$  and  $\phi = \cos^{-1}(2v - 1)$  where  $u$   
 275 and  $v$  are random variates, are utilized for this purpose. To prevent the random points from being  
 276 artificially close to each other (e.g., if two coronae have diameters of 50 km each their centers  
 277 must be  $>100$  km from each other), the ranges of the radii of the randomly generated points are  
 278 chosen to align with the distribution of the radii in the dataset. Each random point is assigned a  
 279 radius value dictated by the probability distribution that best represents the size distribution of  
 280 the dataset to which the random distributions is compared (e.g., a lognormal of the corona  
 281 diameters). The 1st to 99th percentile of the power per degree of the 10,000 iterations are  
 282 extracted, effectively creating a 98% confidence envelope and ignoring potential outliers.  
 283 Spectra with power that falls within the envelope indicates that there would be a less than 1 in  
 284 10,000 chance that they can be distinguished from the spectra of a random population.

285 Comparison of power spectra between two datasets, or between the full population and a  
 286 subset of that population, is performed by obtaining the correlation coefficient per degree,  $r_l$ , of  
 287 two distributions with (Johnson & Richards, 2003; Kirchoff et al., 2011; Richards et al., 1988)

$$288 \quad r_l = \frac{\sum_{m=0}^l (c_{lm}g_{lm} + s_{lm}h_{lm})}{\sqrt{\sum_{m=0}^l (c_{lm}^2 + s_{lm}^2) \sum_{m=0}^l (g_{lm}^2 + h_{lm}^2)}}. \quad (5)$$

289 Correlation values range from -1 to 1. Perfectly positive correlated distributions have a value of  
 290 1, anticorrelations are represented by a value of -1, and distributions with no correlation have a  
 291 value of 0. Further, we use a two-tailed Student-t distribution to calculate the confidence interval  
 292 for a percentage  $t_\alpha$ , with degrees of freedom  $2l$  for the correlation coefficients (Press et al., 1987;  
 293 Wetherill, 1982)

$$294 \quad r_l = \pm t_\alpha \sqrt{\frac{1}{2l + t_\alpha^2}}. \quad (6)$$

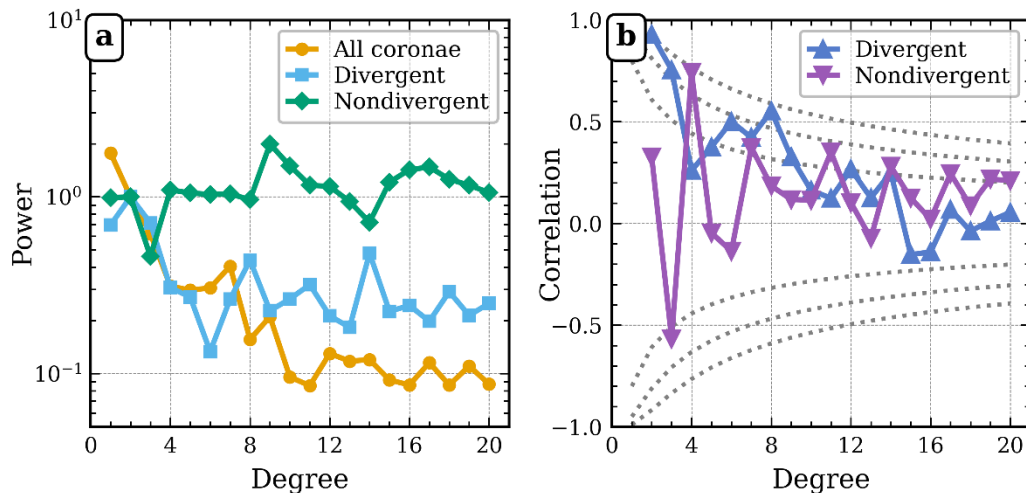
295 Datasets with distributions that are similarly represented by a spherical harmonic degree  
 296 will be strongly correlated at that degree. As discussed by Kirchoff et al. (2011), the lack of  
 297 direct superposition of features does not mean that the features will be anti-correlated, and the  
 298 position of neighboring features affects correlation coefficients at high degrees. Similarly,  
 299 equations (3a) and (3b) ensure that strong correlation will occur at low degrees for similar  
 300 distributions.

301 **3 Results**

302 The locations of volcanoes, coronae, and their subsets are shown in Figure 2, offering a  
 303 qualitative view of their distribution. To quantify these distributions and understand their  
 304 relationships across varying spatial scales, we turn to the analysis of their power spectra. This  
 305 method allows for the exploration of the spatial distribution characteristics of these features and  
 306 their subsets, thereby offering insights into their potential correlations and similarities.

307 The spectra for divergent, nondivergent, and the full population of coronae is shown in  
 308 Figure 4a. We have normalized the spectra to equal 1 at  $l=2$  for easy comparison. The  
 309 nondivergent coronae spectrum is white across all wavelengths, a pattern likely influenced by the  
 310 small sample size ( $N=6$ ). In contrast, the spectra for the full population and the divergent subset  
 311 exhibit similarity at low spherical harmonic degrees, transitioning from a red (decreasing power  
 312 with wavelength to a white (flat) spectrum at higher degrees. This shift suggests a move towards  
 313 a more random or evenly distributed pattern at smaller scales. When examining the correlation at  
 314 low spherical harmonic degrees, we observe a strong relationship between the full corona  
 315 population and the divergent subset, indicating a shared large-scale spatial pattern (Figure 4b).  
 316 However, this correlation weakens at short wavelengths, staying below the 80% confidence level  
 317 for  $l > 14$ .

318



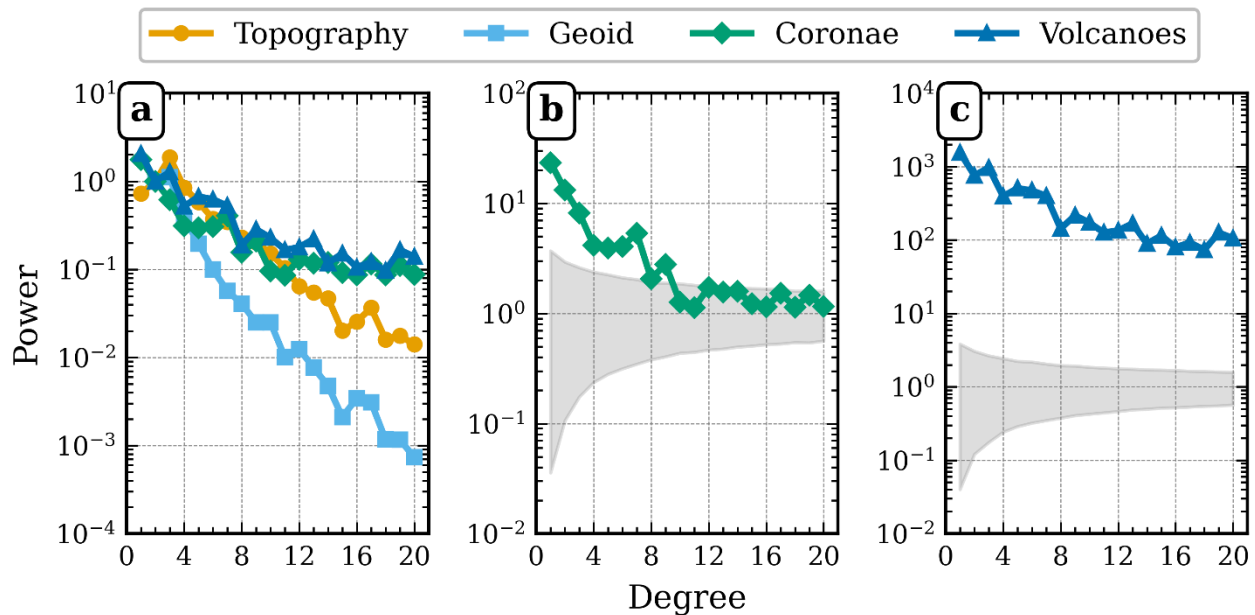
319

320 **Figure 4.** (a) Spectra for the full catalogue and subsets of coronae normalized to equal 1 at  $l=2$ .  
 321 (b) Correlation per degree between all coronae and divergent and nondivergent coronae. Dotted  
 322 lines represent 80%, 95% and 99% confidence intervals, indicating a 20%, 5%, and 1% chance  
 323 of randomness in correlation coefficients for points outside these lines, respectively.

324

325 Figure 5a shows the normalized power spectra of the full catalogues of coronae and  
 326 volcanoes, topography, and geoid. The geoid and topography spectra are red across all  
 327 wavelengths and well correlated visually, consistent with previous studies (e.g., Johnson &  
 328 Richards, 2003; Konopliv et al., 1999; Rappaport et al., 1999; Wieczorek, 2015). Both the full  
 329 datasets of volcanoes and coronae exhibit similar spectral shapes at long wavelengths ( $l < 10$ ),  
 330 transitioning from red to relatively white spectra at higher degrees. However, the volcano  
 331 spectrum's absolute power is approximately two orders of magnitude greater than that of the  
 332 coronae across all wavelengths. Furthermore, the volcano spectrum lies outside of the 99%  
 333 confidence bounds of the 10,000 random distributions (Figure 5c). Both outcomes are likely the  
 334 product of the large number of volcanoes providing good statistical robustness.

335



336

337 **Figure 5.** (a) Normalized spectral power for the full catalogue of coronae (N=545), volcanoes  
 338 (N=85,021), topography, and geoid, set to equal 1 at degree 2 for comparison. Spectra for  
 339 coronae and volcanoes are white at longer wavelengths, whereas topography and geoid remain  
 340 red across all wavelengths shown. Spectral power of (b) coronae and (c) volcanoes without

341 normalizing to degree 2. The grey areas in panels (b) and (c) represent the 1st to 99th percentile  
342 bounds for 10,000 randomly generated samples of coronae and volcanoes, respectively.

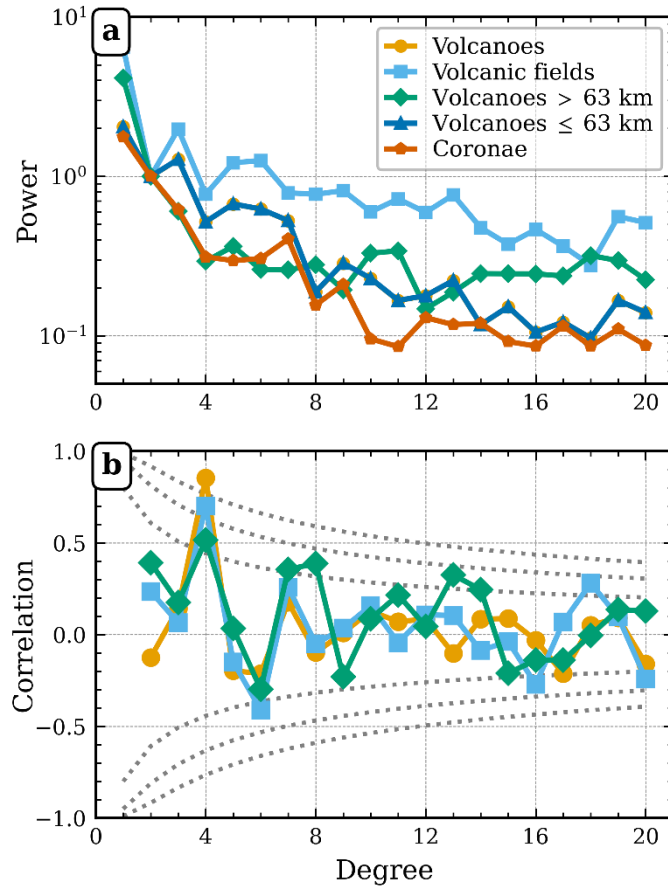
343

344 Figure 6a shows the normalized spectra for all volcanoes, volcanoes  $\leq 63$  km, volcanoes  
345  $> 63$  km, and volcanic fields, which contain high concentrations of shield volcanoes with  
346 diameters  $\leq 20$  km as described by Hahn & Byrne (2023). The population of volcanoes is  
347 dominated by edifices  $\leq 63$  km in diameter. Thus, these data have indistinguishable differences  
348 in the shape of their spectra, and are perfectly positively correlated. As a result, observations  
349 regarding spectra and correlations involving volcanoes  $\leq 63$  km diameter are valid for the  
350 spectrum of the full catalogue. The volcanic fields spectrum shares a similar shape to the full  
351 catalogue, but with less power loss at shorter wavelengths.

352 For volcanoes larger than 63 km in diameter, the spectral pattern diverges at spherical  
353 harmonic degrees greater than 12, becoming relatively blue (power increasing with wavelength).  
354 Given that the minimum diameter of coronae is approximately 60 km, our analysis focuses on  
355 comparing coronae with volcanoes larger than 63 km in diameter. The spectral shapes of these  
356 two datasets exhibit near-identical features at  $l \leq 4$ .

357 In terms of formal correlation, coronae show strong alignment with all subsets of  
358 volcanoes at  $l = 4$ . However, the correlation between coronae and volcanoes  $> 63$  km weakens as  
359 the harmonic degree increases, though it remains above the 80% confidence interval around  $l = 8$   
360 and  $l = 14$ . The minimum diameter of coronae is approximately 60 km. For this reason, we focus  
361 our comparison of corona and volcanoes with those that are  $> 63$  km in diameter. The similarities  
362 in the shape of their spectrum are nearly identical when  $l \leq 4$  (Figure 6a). Coronae are strongly  
363 correlated with volcanoes and volcano subsets at  $l = 4$ . Correlations between volcanoes  $> 63$  km  
364 and coronae weakens with harmonic degree, but is above the 80% confidence interval around  $l =$   
365 8 and  $l = 14$  (Figure 6b).

366



367

368 **Figure 6.** (a) Normalized spectra for coronae and the full catalogue and subsets of volcanoes, set  
 369 to equal 1 at  $l=2$  for comparison. The spectral pattern for the full population of volcanoes closely  
 370 resembles that of volcanoes  $\leq 63$  km ( $N=84,894$ ), which accounts for more than 99% of the total  
 371 population. (b) Correlation between coronae and volcanoes, volcanic fields, and volcanoes  $> 63$   
 372 km. Dotted lines represent 80%, 95% and 99% confidence intervals, indicating a 20%, 5%, and  
 373 1% chance of randomness in correlation coefficients for points outside these lines, respectively.  
 374 The colors in (b) correspond to those in (a).

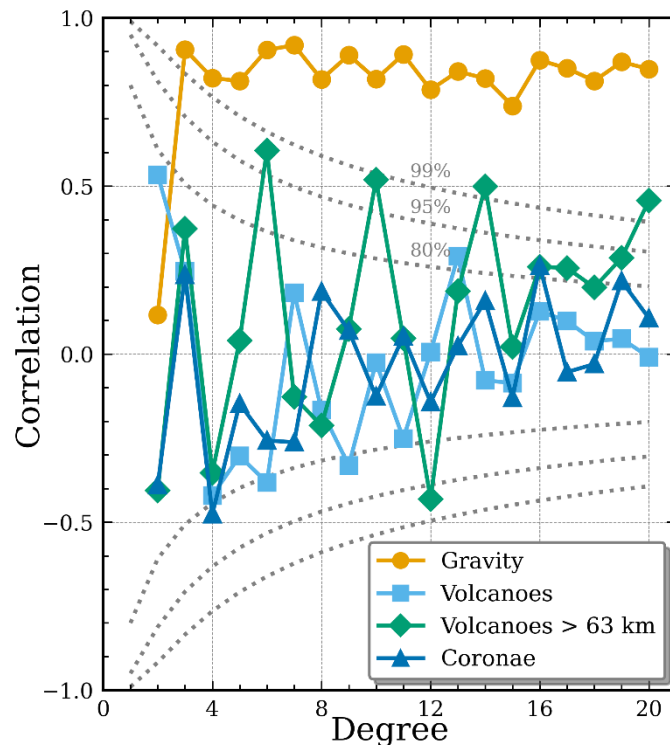
375

#### 376 4 Discussion

377 Venus provides a unique context for investigating the relationship between mantle  
 378 dynamics, surface topography, and volcanic activity. On Earth, the main source of mantle  
 379 circulation is the cooling and sinking of oceanic lithosphere. While mantle plumes have a  
 380 somewhat auxiliary role in Earth's heat budget, they are nonetheless driven by large-scale  
 381 convection in the mantle (e.g., Davies & Richards, 1992; Lay et al., 2008; Sleep, 1990). In  
 382 contrast, Venus may have two modes of mantle plumes: continuous axisymmetric mantle  
 383 upwellings and transient thermals (Johnson & Richards, 2003; Robin et al., 2007). The

384 interaction of the latter with the lithosphere produces the surface expression of a corona,  
 385 although the precise mechanism remains a matter of debate (e.g., Dombard et al., 2007; Gülcher  
 386 et al., 2020; Smrekar and Stofan, 1997; Tucker & Dombard, 2023a). The spectral analysis of the  
 387 spatial distribution of coronae and volcanic features provides valuable insights into these  
 388 complex geodynamic processes. The results have significant implications for our understanding  
 389 of corona formation, the role of volcanic activity, and the broader mantle dynamics on Venus.

390 The lack of correlation between coronae and both topography and gravity on Venus  
 391 (Figure 7) is likely attributable to the coupled nature of large-scale mantle convection and  
 392 transient thermal plumes. Johnson and Richards (2003) proposed that the relative absence of  
 393 coronae in the lowland regions is due to the suppression of transient thermals by broad  
 394 downwelling of cold lithosphere underlying these regions. Further, the concentration of coronae  
 395 in the BAT region, while also being absent from the direct vicinity of active volcanic highlands  
 396 in the BAT region, can be explained by the “capture” of transient thermals by the broad  
 397 upwellings in the region. The correlation between topography and large volcanoes supports this  
 398 hypothesis (Figure 7), as the long-wavelength topography and gravity of Venus are associated  
 399 with large-scale upwelling (e.g., Anderson & Smrekar, 2006; Grimm & Phillips, 1992; Kiefer &  
 400 Hager, 1992; Smrekar, 1994; Smrekar & Phillips, 1991).



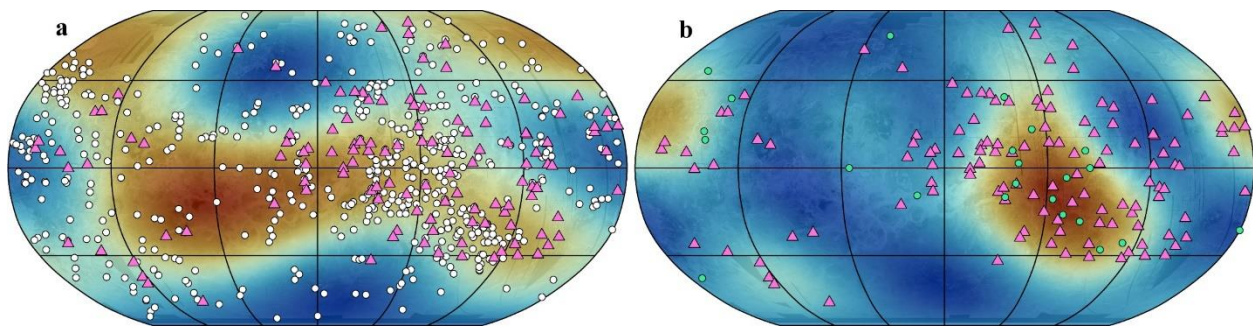
402 **Figure 7.** Correlation between topography and gravity, volcanoes, volcanoes > 63 km, and  
 403 coroneae. Dotted lines represent 80%, 95% and 99% confidence intervals, indicating a 20%, 5%,  
 404 and 1% chance of randomness in correlation coefficients for points outside these lines,  
 405 respectively.

406

407 Aphrodite and Ishtar Terrae are dominant in degrees up to 4 topography (Figure 8). The  
 408 scarcity of volcanoes and coroneae within these highlands contributes to the lack of correlation  
 409 between topography and volcanic features at this spherical harmonic degree. Further, these  
 410 regions explain the significant difference between the spectral power of volcanoes and the  
 411 bounds of the random samples (Figure 5c). The random sampling was not limited by geologic  
 412 boundaries; however, by constraining the latitude range for random sampling from the start to  
 413 sizes comparable to Aphrodite and Ishtar (a computationally inexpensive way to prevent  
 414 sampling from regions), the spectral power increases to a magnitude similar to that for the  
 415 volcano dataset (Supporting Information Figure S1).

416 The dearth of volcanic features observed in these highland plateaus can be ascribed to  
 417 crustal thickening (e.g., James et al., 2013). These compensated highlands may represent old,  
 418 thickened crust making it difficult for plumes to penetrate in these regions (Johnson & Richards,  
 419 2003). Conversely, the strong correlation between volcanic features at  $l = 4$  (Figure 6) is caused  
 420 by the BAT region clustering (Figure 8b).

421



422

423 **Figure 8.** Robinson projected maps, centered at 180°E, of (a) degree 4 truncated spherical  
 424 harmonic expansion of topography where low elevation is represented by blue and red it high  
 425 elevation, and (b) degree 4 truncated representation of the spherical harmonic expansion of the  
 426 full coroneae dataset where blue represents low density and red represents high density regions.  
 427 Both maps are underlain by Magellan SAR mosaic. Pink triangles are locations of volcanoes >63  
 428 km in diameter, white circles (a) are corona locations, and green circles (b) are coroneae with

429 divergent lava flows. The highland plateaus of Aphrodite Terra (60°E-150°E, ~30°S) and Ishtar  
430 Terra (300°E to 60°E, ~75°N) are both largely represented in (a), the degree 4 topography, but  
431 are absent from (b), the degree 4 representation of coronae.

432

433         The spectral analysis of divergent coronae reveals characteristics that align closely with  
434 those of the full population, supporting our assertion that they represent a subset of the  
435 population rather than a distinct group. The concentration of divergent coronae in the BAT  
436 region, consistent with the distribution of the full corona population, further supports this  
437 conclusion. The post-emplacement change in slope direction of lava flows suggests a potential  
438 shift or migration of the magmatic source (Tucker & Dombard, 2023a). Changes in stress  
439 orientations could allow for new pathways for magma ascent, facilitating migration away from  
440 the interior and towards the fracture annulus (e.g., McGovern et al., 2013). The spatial  
441 relationship of these divergent coronae to the complete catalogue, especially their concentration  
442 in the BAT region, implies that this mechanism is integral to their formation rather than being a  
443 consequence of some other regional or random phenomenon. The “white” spectrum and lack of  
444 correlation seen in nondivergent coronae (Figure 8) is likely due to the small sample size.  
445 However, the limited number of observed nondivergent coronae reinforces our interpretation that  
446 this process is an intrinsic part of corona formation.

447         The relationship between volcanism and coronae is well established (e.g., Head et al.,  
448 1992; Roberts & Head, 1993). With few exceptions, the magmatic relationship is rarely  
449 explicitly incorporated in geophysical models of formation (e.g., Dombard et al., 2007; Lang &  
450 López, 2015), instead focusing on the dynamics of the plume-lithosphere interaction. In addition  
451 to observations of volcanism at coronae, the long wavelength spectral similarities between  
452 coronae and volcanoes > 63 km suggest that they are influenced by the same long-wavelength  
453 mantle dynamics.

454         In addition to the direct observations of volcanic activity at coronae, the spectral analysis  
455 reveals similarities between coronae and large volcanoes. Specifically, the long-wavelength  
456 spectral characteristics of these features exhibit similar trends as well as correlation (> 80%  
457 confidence) at various long-wavelength scales. This correlation is further strengthened by the  
458 observed clustering of coronae and large volcanoes in the BAT region. The patterns observed  
459 align well with models that invoke mantle material upwelling and its interaction with the

460 lithosphere, resulting in volcanic activity and surface deformation. The strong correlation at low  
461 spherical harmonic degrees and shared spatial distribution underline a likely commonality in the  
462 mantle processes that drive coronae formation.

## 463 **5 Conclusion**

464 Observations of coronae from SAR images show many associated volcanic features and  
465 landforms. By mapping discrete lava flows within corona fracture annuli, we have developed a  
466 new subset of the corona dataset of coronae with topography that has changed since the  
467 emplacement of those lava flows. Spectral power analysis of the distribution of divergent  
468 coronae shows that they are a part of the same distribution of the full population of coronae,  
469 rather than a random or regional occurrence. Furthermore, coronae have a strong correlation and  
470 spectral shape at low spherical harmonic degrees with volcanoes of comparable scale suggesting  
471 a shared geodynamic origin.

472 These observations underscore the significance of volcanism and highlight the need for  
473 future investigations that incorporate magmatic processes into models of corona formation,  
474 instead of models that ascribe coronae as the products of plume/lithosphere interactions. As with  
475 many studies that rely on surface observations of Venus, improved resolution of surface SAR  
476 imagery, topography, and gravity data would further refine our understanding of the geologic  
477 and geophysical processes related to coronae and volcanism. Improved data would likely  
478 increase the number of coronae at which divergent lava flows due to better identification of flow  
479 margins. Additionally, it would allow for measurements of flow divergence to be better  
480 constrained.

## 481 **Acknowledgments**

482 Portions of this work were funded by the Illinois Space Grant Consortium. Early portions of this  
483 work were presented at the Lunar and Planetary Science Conference with support from the  
484 University of Illinois Chicago LAS Travel Award.

## 485 **Open Research**

486 The global catalog of volcanoes developed by Hahn and Byrne (2023) is available  
487 through the Washington University in St. Louis Open Scholarship repository (Hahn & Byrne,

488 2022). The Stofan et al. (2001a) catalogue of Type 1 and Type 2 coronae is available through the  
 489 NASA Planetary Data System (Stofan et al., 2001b). NASA Magellan Mission data, including  
 490 full-resolution and compressed SAR images (Pettengill, 1991) and global topography data (Ford,  
 491 1992), and stereo-derived topography data (Herrick, 2020) is available from the NASA Planetary  
 492 Data System. A portion of the spherical harmonic calculations were performed using SHTools  
 493 (Wieczorek & Meschede, 2018). The Venus topography model, VenusTopo719 (Wieczorek,  
 494 2015), and gravity model, MGNP180U (Konopliv et al., 1999), are available through the  
 495 *datasets* submodule in SHTools. The Python code SHPointPower for the spherical harmonic  
 496 analysis is available via GitHub (Tucker, 2023), and GIS shapefiles of the mapped lava flow  
 497 centerlines are available via Zenodo (Tucker & Dombard, 2023b).

498

499 **References**

- 500 Anderson, F. S., & Smrekar, S. E. (2006). Global mapping of crustal and lithospheric thickness  
 501 on Venus. *Journal of Geophysical Research*, *111*(8), 1–20.  
 502 <https://doi.org/10.1029/2004JE002395>
- 503 Arvidson, R. E., Greeley, R., Malin, M. C., Saunders, R. S., Izenberg, N., Plaut, J. J., et al.  
 504 (1992). Surface modification of Venus as inferred from Magellan observations of plains.  
 505 *Journal of Geophysical Research*, *97*(E8), 13303. <https://doi.org/10.1029/92JE01384>
- 506 Aubele, J. C., & Slyuta, E. N. (1990). Small domes on Venus: Characteristics and origin. *Earth,*  
 507 *Moon and Planets*, *50–51*(1), 493–532. <https://doi.org/10.1007/BF00142404>
- 508 Barsukov, V. L., Basilevsky, A. T., Burba, G. A., Bobinna, N. N., Kryuchkov, V. P., Kuzmin, R.  
 509 O., et al. (1986). The geology and geomorphology of the Venus surface as revealed by  
 510 the radar images obtained by Veneras 15 and 16. *Journal of Geophysical Research*,  
 511 *91*(B4), 378–398. <https://doi.org/10.1029/JB091iB04p0D378>
- 512 Bindschadler, D. L., Schubert, G., & Kaula, W. M. (1992). Coldspots and hotspots: Global  
 513 tectonics and mantle dynamics of Venus. *Journal of Geophysical Research*, *97*(E8),  
 514 13495. <https://doi.org/10.1029/92JE01165>
- 515 Copp, D. L., Guest, J. E., & Stofan, E. R. (1998). New insights into Coronae evolution: Mapping  
 516 on Venus. *Journal of Geophysical Research*, *103*(E8), 19401–19417.  
 517 <https://doi.org/10.1029/97JE03182>
- 518 Davaille, A., Smrekar, S. E., & Tomlinson, S. (2017). Experimental and observational evidence  
 519 for plume-induced subduction on Venus. *Nature Geoscience*, *10*(5), 349–355.  
 520 <https://doi.org/10.1038/ngeo2928>
- 521 Davies, G. F., & Richards, M. A. (1992). Mantle Convection. *The Journal of Geology*, *100*(2).  
 522 <https://doi.org/https://doi.org/10.1086/629582>

- 523 DeLaughter, J. E., & Jurdy, D. M. (1999). Corona Classification by Evolutionary Stage. *Icarus*,  
524 139(1), 81–92. <https://doi.org/10.1006/icar.1999.6087>
- 525 Dombard, A. J., Johnson, C. L., Richards, M. A., & Solomon, S. C. (2007). A magmatic loading  
526 model for coronae on Venus. *Journal of Geophysical Research*, 112(4), 1–13.  
527 <https://doi.org/10.1029/2006JE00273>
- 528 Ford, P. G. (1992). MGN V RDRS 5 global data record topographic V1.0 [Dataset]. NASA  
529 Planetary Data System. <https://doi.org/10.17189/1522522>
- 530 Gerya, T. V. (2014). Plume-induced crustal convection: 3D thermomechanical model and  
531 implications for the origin of novae and coronae on Venus. *Earth and Planetary Science*  
532 *Letters*, 391, 183–192. <https://doi.org/10.1016/j.epsl.2014.02.005>
- 533 Glaze, L. S., Stofan, E. R., Smrekar, S. E., & Baloga, S. M. (2002). Insights into corona  
534 formation through statistical analyses. *Journal of Geophysical Research*, 107(E12), 18-1-  
535 18–12. <https://doi.org/10.1029/2002JE001904>
- 536 Grimm, R. E., & Phillips, R. J. (1992). Anatomy of a Venusian hot spot: Geology, gravity, and  
537 mantle dynamics of Eistla Regio. *Journal of Geophysical Research*, 97(E10), 16035.  
538 <https://doi.org/10.1029/92JE01500>
- 539 Guest, J. E., Bulmer, M. H., Aubele, J. C., Beratan, K. K., Greeley, R., Head, J. W., et al. (1992).  
540 Small volcanic edifices and volcanism in the plains of Venus. *Journal of Geophysical*  
541 *Research: Planets*, 97(E10), 15949–15966. <https://doi.org/10.1029/92JE01438>
- 542 Guest, J. E., & Stofan, E. R. (1999). A New View of the Stratigraphic History of Venus. *Icarus*,  
543 139(1), 55–66. <https://doi.org/10.1006/icar.1999.6091>
- 544 Gülcher, A. J. P., Gerya, T. V., Montési, L. G. J., & Munch, J. (2020). Corona structures driven  
545 by plume–lithosphere interactions and evidence for ongoing plume activity on Venus.  
546 *Nature Geoscience*, 13(8), 547–554. <https://doi.org/10.1038/s41561-020-0606-1>
- 547 Hahn, R. M., & Byrne, P. K. (2022). A global catalog of volcanoes and volcanic fields on Venus  
548 [V2] (version 2) [Dataset]. Washington University in St. Louis.  
549 <https://doi.org/10.7936/8XY0-X885>
- 550 Hahn, R. M., & Byrne, P. K. (2023). A Morphological and Spatial Analysis of Volcanoes on  
551 Venus. *Journal of Geophysical Research: Planets*, 128(4), 1–26.  
552 <https://doi.org/10.1029/2023JE007753>
- 553 Hansen, V. L. (2002). Artemis: Surface expression of a deep mantle plume on Venus. *Bulletin of*  
554 *the Geological Society of America*, 114(7), 839–848. [https://doi.org/10.1130/0016-7606\(2002\)114<0839:ASEOAD>2.0.CO;2](https://doi.org/10.1130/0016-7606(2002)114<0839:ASEOAD>2.0.CO;2)
- 556 Hauck, S. A. I., Phillips, R. J., & Price, M. H. (1998). Venus: Crater distribution and plains  
557 resurfacing models. *Journal of Geophysical Research: Planets*, 103(E6), 13635–13642.  
558 <https://doi.org/10.1029/98JE00400>
- 559 Head, J. W., Crumpler, L. S., Aubele, J. C., Guest, J. E., & Saunders, R. S. (1992). Venus  
560 volcanism: Classification of volcanic features and structures, associations, and global  
561 distribution from Magellan data. *Journal of Geophysical Research*, 97(E8), 13153.  
562 <https://doi.org/10.1029/92JE01273>

- 563 Herrick, R. R. (2020). Magellan Venus stereo-derived topography Bundle. [Dataset].  
564 Geosciences Node. <https://doi.org/https://doi.org/10.17189/1519332>
- 565 Herrick, R. R., & Hensley, S. (2023). Direct Observation of Volcanic Activity on Venus from  
566 Repeat Magellan Imaging. In L. and P. Institute (Ed.), *54th Lunar and Planetary Science*  
567 *Conference*. Retrieved from <https://www.hou.usra.edu/meetings/lpsc2023/pdf/1061.pdf>
- 568 Herrick, R. R., & Sharpton, V. L. (2000). Implications from stereo-derived topography of  
569 Venusian impact craters. *Journal of Geophysical Research: Planets*, *105*(E8), 20245–  
570 20262. <https://doi.org/10.1029/1999JE001225>
- 571 Herrick, R. R., Sharpton, V. L., Malin, M. C., Lyons, S. N., & Feely, K. (1997). Morphology and  
572 Morphometry of Impact Craters. In S. W. Bougher, D. M. Hunten, R. J. Phillips (Eds.),  
573 *Venus II: Geology, Geophysics, Atmosphere, and Solar Wind Environment* (pp. 1015–  
574 1046). Tucson, AZ: The University of Arizona Press.
- 575 Herrick, R. R., Stahlke, D. L., & Sharpton, V. L. (2012). Fine-scale Venusian topography from  
576 Magellan stereo data. *Eos, Transactions American Geophysical Union*, *93*(12), 125–126.  
577 <https://doi.org/10.1029/2012EO120002>
- 578 Hoogenboom, T., & Houseman, G. A. (2006). Rayleigh-Taylor instability as a mechanism for  
579 corona formation on Venus. *Icarus*, *180*(2), 292–307.  
580 <https://doi.org/10.1016/j.icarus.2005.11.001>
- 581 Ivanov, M. A., Crumpler, L. S., Aubele, J. C., & Head, J. W. (2015). Volcanism on Venus. In H.  
582 Sigurdsson (Ed.), *The Encyclopedia of Volcanoes* (Second Edi, pp. 729–746). Academic  
583 Press. <https://doi.org/10.1016/B978-0-12-385938-9.00042-0>
- 584 James, P. B., Zuber, M. T., & Phillips, R. J. (2013). Crustal thickness and support of topography  
585 on Venus. *Journal of Geophysical Research: Planets*, *118*(4), 859–875.  
586 <https://doi.org/10.1029/2012JE004237>
- 587 Janes, D. M., & Squyres, S. W. (1995). Viscoelastic relaxation of topographic highs on Venus to  
588 produce coronae. *Journal of Geophysical Research*, *100*(E10), 21173.  
589 <https://doi.org/10.1029/95je01748>
- 590 Jellinek, A. M., Lenardic, A., & Manga, M. (2002). The influence of interior mantle temperature  
591 on the structure of plumes: Heads for Venus, Tails for the Earth. *Geophysical Research*  
592 *Letters*, *29*(11), 1532. <https://doi.org/10.1029/2001GL014624>
- 593 Johnson, C. L., & Richards, M. A. (2003). A conceptual model for the relationship between  
594 coronae and large-scale mantle dynamics on Venus. *Journal of Geophysical Research*,  
595 *108*(6), 5058. <https://doi.org/10.1029/2002je001962>
- 596 Kiefer, W. S., & Hager, B. H. (1992). Geoid anomalies and dynamic topography from  
597 convection in cylindrical geometry: applications to mantle plumes on Earth and Venus.  
598 *Geophysical Journal International*, *108*(1), 198–214. [https://doi.org/10.1111/j.1365-](https://doi.org/10.1111/j.1365-246X.1992.tb00850.x)  
599 [246X.1992.tb00850.x](https://doi.org/10.1111/j.1365-246X.1992.tb00850.x)
- 600 Kirchoff, M. R., McKinnon, W. B., & Schenk, P. M. (2011). Global distribution of volcanic  
601 centers and mountains on Io: Control by asthenospheric heating and implications for  
602 mountain formation. *Earth and Planetary Science Letters*, *301*(1–2), 22–30.  
603 <https://doi.org/10.1016/j.epsl.2010.11.018>

- 604 Koch, D. M., & Manga, M. (1996). Neutrally buoyant diapirs: A model for Venus coronae.  
605 *Geophysical Research Letters*, 23(3), 225–228. <https://doi.org/10.1029/95GL03776>
- 606 Konopliv, A. S., Banerdt, W. B., & Sjogren, W. L. (1999). Venus Gravity: 180th Degree and  
607 Order Model. *Icarus*, 139(1), 3–18. <https://doi.org/10.1006/icar.1999.6086>
- 608 Lang, N. P., & López, I. (2015). The magmatic evolution of three Venusian coronae. *Geological*  
609 *Society, London, Special Publications*, 401(1), 77–95. <https://doi.org/10.1144/SP401.3>
- 610 Lay, T., Hernlund, J., & Buffett, B. A. (2008). Core–mantle boundary heat flow. *Nature*  
611 *Geoscience*, 1(1), 25–32. <https://doi.org/10.1038/ngeo.2007.44>
- 612 McGovern, P. J., Rumpf, M. E., & Zimbelman, J. R. (2013). The influence of lithospheric  
613 flexure on magma ascent at large volcanoes on Venus. *Journal of Geophysical Research:*  
614 *Planets*, 118(11), 2423–2437. <https://doi.org/10.1002/2013JE004455>
- 615 McKenzie, D., Ford, P. G., Johnson, C. L., Parsons, B., Sandwell, D. T., Saunders, R. S., &  
616 Solomon, S. C. (1992). Features on Venus generated by plate boundary processes.  
617 *Journal of Geophysical Research*, 97(E8), 13533. <https://doi.org/10.1029/92JE01350>
- 618 McKinnon, W. B., Zahnle, K. B., Ivanov, B. A., & Melosh, H. J. (1997). Cratering on Venus. In  
619 S. W. Bougher, D. M. Hunten, & R. J. Phillips (Eds.), *Venus II: Geology, Geophysics,*  
620 *Atmosphere, and Solar Wind Environment* (pp. 969–1014). Tucson, AZ: The University  
621 of Arizona Press.
- 622 Pettengill, G. (1991) MGN V RDRS derived mosaic image data record full res (V1.0 [Dataset].  
623 NASA Planetary Data System. <https://doi.org/10.17189/1522523>
- 624 Phillips, R. J., & Malin, M. C. (1983). The interior of Venus and tectonic implications. In D. M.  
625 Hunten, L. Colin, T. M. Donahue, & V. I. Moroz (Eds.), *Venus* (pp. 159–214). Tucson,  
626 AZ: The University of Arizona Press.  
627 <https://doi.org/https://doi.org/10.2307/j.ctv25c4z16>.
- 628 Phillips, R. J., Raubertas, R. F., Arvidson, R. E., Sarkar, I. C., Herrick, R. R., Izenberg, N., &  
629 Grimm, R. E. (1992). Impact Craters and Venus Resurfacing History. *Journal of*  
630 *Geophysical Research*, 97(E10), 15923. <https://doi.org/10.1029/92JE01696>
- 631 Rappaport, N. J., Konopliv, A. S., Kucinskis, A. B., & Ford, P. G. (1999). An Improved 360  
632 Degree and Order Model of Venus Topography. *Icarus*, 139(1), 19–31.  
633 <https://doi.org/10.1006/icar.1999.6081>
- 634 Ribe, N. M., & de Valpine, D. P. (1994). The global hotspot distribution and instability of D".  
635 *Geophysical Research Letters*, 21(14), 1507–1510. <https://doi.org/10.1029/94GL01168>
- 636 Richards, M. A., Hager, B. H., & Sleep, N. H. (1988). Dynamically supported geoid highs over  
637 hotspots: observation and theory. *Journal of Geophysical Research*, 93(B7), 7690–7708.  
638 <https://doi.org/10.1029/JB093iB07p07690>
- 639 Roberts, K. M., & Head, J. W. (1993). Large-scale volcanism associated with coronae on Venus:  
640 Implications for formation and evolution. *Geophysical Research Letters*, 20(12), 1111–  
641 1114. <https://doi.org/10.1029/93GL01484>
- 642 Robin, C. M. I., Jellinek, A. M., Thayalan, V., & Lenardic, A. (2007). Transient mantle  
643 convection on Venus: The paradoxical coexistence of highlands and coronae in the BAT

- 644 region. *Earth and Planetary Science Letters*, 256(1–2), 100–119.  
645 <https://doi.org/10.1016/j.epsl.2007.01.016>
- 646 Russell, M. B., & Johnson, C. L. (2021). Evidence for a Locally Thinned Lithosphere Associated  
647 with Recent Volcanism at Aramaiti Corona, Venus. *Journal of Geophysical Research:*  
648 *Planets*, 126(8), 1–19. <https://doi.org/10.1029/2020JE006783>
- 649 Sandwell, D. T., & Schubert, G. (1992). Evidence for Retrograde Lithospheric Subduction on  
650 Venus. *Science*, 257(5071), 766–770. <https://doi.org/10.1126/science.257.5071.766>
- 651 Schaber, G. G., Strom, R. G., Moore, H. J., Soderblom, L. A., Kirk, R. L., Chadwick, J., et al.  
652 (1992). Geology and distribution of impact craters on Venus: What are they telling us?  
653 *Journal of Geophysical Research*, 97(E8), 13257. <https://doi.org/10.1029/92JE01246>
- 654 Silverman, B. W. (1998). *Density Estimation for Statistics and Data Analysis*. Routledge.  
655 <https://doi.org/10.2307/2347507>
- 656 Sleep, N. H. (1990). Hotspots and mantle plumes: Some phenomenology. *Journal of*  
657 *Geophysical Research*, 95(B5), 6715. <https://doi.org/10.1029/JB095iB05p06715>
- 658 Slyuta, E. N. (1990). Large Shield Volcanoes (>100 Km in Diameter) on Venus: Morphologic  
659 Types. In *21st Lunar and Planetary Science Conference*. Retrieved from  
660 <https://articles.adsabs.harvard.edu/full/1990LPI....21.1172S>
- 661 Slyuta, E. N., & Kreslavsky, M. A. (1990). Intermediate (20-100 Km) Sized Volcanic Edifices  
662 on Venus. In *21st Lunar and Planetary Science Conference*. Retrieved from  
663 <https://articles.adsabs.harvard.edu/full/1990LPI....21.1174S>
- 664 Smrekar, S. E. (1994). Evidence for Active Hotspots on Venus from Analysis of Magellan  
665 Gravity Data. *Icarus*, 112(1), 2–26. <https://doi.org/10.1006/icar.1994.1166>
- 666 Smrekar, S. E., Davaille, A., & Sotin, C. (2018). *Venus Interior Structure and Dynamics*. *Space*  
667 *Science Reviews* (Vol. 214). Springer Nature B.V. [https://doi.org/10.1007/s11214-018-](https://doi.org/10.1007/s11214-018-0518-1)  
668 0518-1
- 669 Smrekar, S. E., Kiefer, W. S., & Stofan, E. R. (1997). Large volcanic rises on Venus. In S. W.  
670 Bougher, D. M. Hunten, & R. J. Phillips (Eds.), *Venus II: Geology, Geophysics,*  
671 *Atmosphere, and Solar Wind Environment* (pp. 845–878). Tucson, AZ: University of  
672 Arizona Press.
- 673 Smrekar, S. E., & Phillips, R. J. (1991). Venusian highlands: geoid to topography ratios and their  
674 implications. *Earth and Planetary Science Letters*, 107(3–4), 582–597.  
675 [https://doi.org/10.1016/0012-821X\(91\)90103-O](https://doi.org/10.1016/0012-821X(91)90103-O)
- 676 Smrekar, S. E., & Stofan, E. R. (1999). Origin of Corona-Dominated Topographic Rises on  
677 Venus. *Icarus*, 139(1), 100–115. <https://doi.org/10.1006/icar.1999.6090>
- 678 Smrekar, S. E., Stofan, E. R., Mueller, N., Treiman, A. H., Elkins-Tanton, L. T., Helbert, J., et al.  
679 (2010). Recent hotspot volcanism on Venus from VIRTIS emissivity data. *Science*,  
680 328(5978), 605–608. <https://doi.org/10.1126/science.1186785>
- 681 Squyres, S. W., Janes, D. M., Baer, G., Bindschadler, D. L., Schubert, G., Sharpton, V. L., &  
682 Stofan, E. R. (1992). The morphology and evolution of coronae on Venus. *Journal of*  
683 *Geophysical Research*, 97(E8), 13611. <https://doi.org/10.1029/92je01213>

- 684 Squyres, S. W., Janes, D. M., Schubert, G., Bindschadler, D. L., Moersch, J. E., Turcotte, D. L.,  
685 & Stofan, E. R. (1993). The spatial distribution of coronae and related features on Venus.  
686 *Geophysical Research Letters*, 20(24), 2965–2968. <https://doi.org/10.1029/93GL00866>
- 687 Stofan, E. R., Hamilton, V. E., Janes, D. M., & Smrekar, S. E. (1997). Coronae on Venus:  
688 Morphology and Origin. In S. W. Bougher, D. M. Hunten, & R. J. Phillips (Eds.), *Venus*  
689 *II: Geology, Geophysics, Atmosphere, and Solar Wind Environment* (pp. 931–965).  
690 Tucson, AZ: University of Arizona Press. <https://doi.org/10.2307/j.ctv27tct5m>
- 691 Stofan, E. R., Sharpton, V. L., Schubert, G., Baer, G., Bindschadler, D. L., Janes, D. M., &  
692 Squyres, S. W. (1992). Global distribution and characteristics of coronae and related  
693 features on Venus: Implications for origin and relation to mantle processes. *Journal of*  
694 *Geophysical Research*, 97(E8), 13347. <https://doi.org/10.1029/92JE01314>
- 695 Stofan, E. R., Smrekar, S. E., Bindschadler, D. L., & Senske, D. A. (1995). Large topographic  
696 rises on Venus: Implications for mantle upwelling. *Journal of Geophysical Research*,  
697 100(E11), 23317. <https://doi.org/10.1029/95JE01834>
- 698 Stofan, E. R., Smrekar, S. E., Tapper, S. W., Guest, J. E., & Grindrod, P. M. (2001a).  
699 Preliminary analysis of an expanded corona database for Venus. *Geophysical Research*  
700 *Letters*, 28(22), 4267–4270. <https://doi.org/10.1029/2001GL013307>
- 701 Stofan, E. R., Smrekar, S. E., Tapper, S. W., Guest, J. E., & Grindrod, P. M. (2001b).  
702 Preliminary analysis of an expanded corona database for Venus. NASA Planetary Data  
703 System. <https://pdsimage2.wr.usgs.gov/pub/pigpen/venus/Coronae/>
- 704 Strom, R. G., Schaber, G. G., & Dawson, D. D. (1994). The global resurfacing of Venus. *Journal*  
705 *of Geophysical Research*, 99(E5), 10,899–10,926. <https://doi.org/10.1029/94JE00388>
- 706 Tucker, W. S. (2023). *SHPointPower* (v1.0.0) [Software]. Zenodo.  
707 <https://doi.org/10.5281/zenodo.10084438>
- 708 Tucker, W. S. & Dombard, A. J. (2023a). Evidence of Topographic Change Recorded by Lava  
709 Flows at Atete and Aruru Coronae on Venus. *Journal of Geophysical Research: Planets*,  
710 128, e2023JE007971. <https://doi.org/10.1029/2023JE007971>
- 711 Tucker, W. S. & Dombard, A. J. (2023b) SI files for Spherical-harmonic distribution of coronae  
712 in relation to volcanic features on Venus. [Dataset]. Zenodo.  
713 <https://doi.org/10.5281/zenodo.10144166>
- 714 Wieczorek, M. A. (2015). Gravity and topography of the terrestrial planets. In G. Schubert & T.  
715 Spohn (Eds.), *Treatise on Geophysics* (2nd ed., Vol. 10, pp. 153–193). Oxford, UK:  
716 Elsevier-Pergamon. <https://doi.org/10.1016/B978-0-444-53802-4.00169-X>
- 717 Wieczorek, M. A., & Meschede, M. (2018). SHTools: Tools for Working with Spherical  
718 Harmonics. *Geochemistry, Geophysics, Geosystems*, 19(8), 2574–2592.  
719 <https://doi.org/10.1029/2018GC007529>
- 720